Available online at www.sciencedirect.com

Manufacturing Letters

Manufacturing Letters 41 (2024) 862–867

52nd SME North American Manufacturing Research Conference (NAMRC 52, 2024)

Rapid 3D printing of electro-active hydrogels

Wenbo Wang[a], Siying Liu[a], Mingqi Yu[a], Xiangfan Chen[a]*

[a]*School of Manufacturing Systems and Networks, Arizona State University, Mesa, AZ 85212, US*

* Corresponding author. Tel.: +1-480-727-2662. *E-mail address:* xiangfan.chen@asu.edu

Abstract

Electroactive hydrogels (EAH) have gained prominence for their unique ability to change shape or size under an electric field, finding applications in biosensors and soft actuators. This study focuses on a tunnelable EAH tailored for high-resolution 3D printing via the micro continuous liquid interface production (μCLIP) process. The resin formulations mainly involve acrylic acid (AA) and 4-hydroxybutyl acrylate (4-HBA). AA, with its carboxyl groups, introduces electroactuation, generating osmotic pressure in the hydrogel matrix. This results in swelling, inducing bending towards the cathode, accentuating the material's responsiveness. In contrast, 4-HBA offers mechanical resilience, providing an elastic backbone, and ensuring the hydrogel's applicability. Our results illustrate the hydrogel's strength, flexibility, and bending capabilities across varied compositions and electric field strengths. Notably, the μCLIP process enabled the 3D printing of our EAH into sophisticated structures, like the lattice. The combination of AA's electro-responsive traits with 4-HBA's durability has birthed a material with vast practical implications. This study provides extended potential breakthroughs in soft robotics, wearable electronics, and medical devices, marking a significant stride in the realm of electroactive materials.

Peer-review under responsibility of the scientific committee of the NAMRI/SME.
Keywords: 3D printing, μCLIP, electroactive hydrogel, soft actuator

1. Introduction

Soft actuators, characterized by their exceptional deformability and responsiveness to various external stimuli including light, pH, heat, humidity, and electric/magnetic fields, represent a cutting-edge frontier in materials science and engineering [1]. These remarkable materials can be triggered to generate specific motions and forces/torques through intricate mechanisms involving volume change or shape deformation, driven by subtle microscopic changes within the material [2].

Particularly, electroactive hydrogels (EAHs) have been at the forefront of research within the realm of smart materials due to their unique ability to undergo significant deformation in response to external electrical stimuli [3]. With potential applications ranging from soft robotics to biomedical devices, EAHs hold great promise for the future [4]. The primary mechanism underpinning the behavior of EAHs is electro-osmotic interactions within their matrix. Ion migration, induced by an electric field, results in osmotic pressure differences and subsequent swelling or deswelling of the hydrogel [5]. Such controlled deformation positions EAHs as efficient candidates for actuators in microdevices and responsive drug delivery systems [3].

However, despite their potential, a primary challenge that persists is achieving a balance between the hydrogel's electroactivity and its mechanical robustness. While various studies have documented the desirable electroactive behavior of EAHs, many such materials lack the mechanical resilience needed for wider practical applications [6]. This has spurred a quest for innovative materials and fabrication methods that can offer both high electroactivity and versatile mechanical strength.

Recent advancements in fabrication techniques, particularly micro continuous liquid interface production (μCLIP), a high-resolution 3D printing method, have shown promise in the rapid fabrication of hydrogels into sophisticated structures [7]. By

Peer-review under responsibility of the scientific committee of the NAMRI/SME.

facilitating the precise structuring of hydrogels, this method potentially enhances both their mechanical and electroactive attributes. To prepare the photoresins for vat-polymerization, acrylic acid (AA), due to its inherent electro actuation capabilities stemming from its carboxyl groups, has emerged as a preferred choice in many studies [8], [9]. In tandem, 4-hydroxybutyl acrylate (4-HBA) has been identified as a valuable monomer for its potential to alter hydrogel mechanical properties without significantly compromising electroactivity, with its addition also increasing the deformability of the printed EAH [10], [11]. By carefully adjusting the relative ratio between AA and 4-HBA, the mechanical behavior of the printed EAH can be effectively tuned to suit a variety of applications.

In this study, we advance the current state of the art by investigating the fabrication of EAHs via μCLIP using the combination of AA and 4-HBA (Figure 1). Our assessment of various compositions seeks to elucidate their impact on hydrogel attributes. By optimizing printing parameters, high-resolution, intricate structures could be efficiently produced using μCLIP. We evaluated EAHs made with different AA and 4-HBA concentrations to discern the relationship between their compositions and mechanical strength. A thorough analysis of the electro-actuation performance provided insights into how resin compositions influence mechanical robustness. This work aims to set the foundation for creating EAHs tailored for diverse applications.

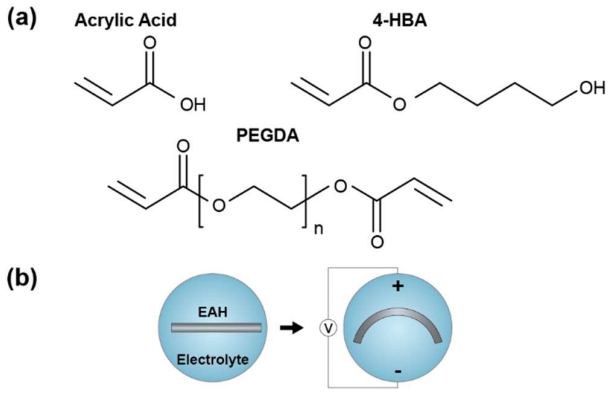

Figure 1. (a) Chemical structures of major materials; (b) Bending mechanism of EAH actuators.

2. Materials and Methods

2.1. Materials and Preparation of the photocurable resin

Acrylic Acid (AA, 99%), poly(ethylene glycol) diacrylate (PEGDA) (average Mn 700), phenylbis(2,4,6-trimethylbenzoyl)phosphine oxide (Irgacure 819, 97+%), and 2-(2H-Benzotriazol-2-yl)-6-dodecyl-4-methylphenol (Tinuvin 171) were purchased from Sigma-Aldrich. 4-hydroxybutyl acrylate (4-HBA, 97%+), ACS grade deionized water (DI), and phosphate buffered saline (PBS, 1×) were purchased from Fisher Scientific. All chemicals were used as received without further modifications.

A series of photocurable resins containing varying concentrations of AA were prepared, with the detailed compositions are listed in Table 1. To prepare the photocurable resins suitable for μCLIP, corresponding AA and 4-HBA content was mixed, followed by adding 2 wt.% of PEGDA as crosslinker, 2 wt.% of Irgacure 819 as UV photoinitiator, and 1 wt.% of Tinuvin 171 as photoabsorber. The resulting resin was then sonicated for one hour before conducting printing, and all synthesis processes were performed in a dark environment.

Table 1. List of resins and compositions.

Entry	AA (wt.%)	4-HBA (wt.%)
1	70	25
2	50	45
3	30	65

2.2. EAH fabrication via micro continuous liquid interface production (μCLIP)

A home-built μCLIP system was utilized to fabricate the EAH (Figure 2a). To prepare the printing file, CAD models were sliced with a layer thickness of 5 μm into serial mask images using a customized slicing program. The mask images were sequentially projected through a light engine (Pro4500, Wintech Digital) equipped with a digital micromirror device (DMD) with a resolution of 1280 × 800 and a UV light source with a center wavelength of 405 nm. The projection was focused into the resin bath through a UV lens (UV8040BK2, Universe Optics) with a final pixel resolution of 5.6 × 5.6 μm. To yield the polymerization-free zone (dead zone), an oxygen-permeable membrane (Teflon AF2400, 70 μm nominal thickness, Biogeneral) was utilized to introduce oxygen molecules as free-radical scavengers. A CMOS camera (MU2993-BI, AmScope) was applied to assist in focusing and monitoring the projection on the membrane. The light intensity at the focal plane was fixed at 1.16 mW/cm^2 throughout this study. To lift the printing platform vertically during the bottom-up printing process, a high-resolution linear motorized stage (XLSM200A, Zaber Technology Inc.) was deployed as the z-axis. Each component was controlled with a customized computer program to conduct the 3D printing.

2.3. Characterization of mechanical strength

The mechanical strength of EAHs printed with each resin was measured on a dynamic mechanical analysis (DMA) (Discover Hybrid HR2, TA Instruments). For the tensile tests, dog bone samples were designed with a gauge length of 3 mm, gauge width of 1 mm, gripping length of 5 mm, gripping width of 5 mm, and thickness of 0.5 mm (Figure 3a). Samples were prepared with μCLIP, followed by rinsing with IPA to remove residual resin and post-curing with UV irradiation for 30 min. A strain rate of 300 μm·s^{-1} was applied for all tensile tests.

2.4. Characterization of EAH performance

To assess the underwater actuation performance of the fabricated EAHs, an electrolyte solution was prepared by diluting PBS with DI water, resulting in a 0.05 M PBS solution.

After printing, the samples underwent a rinse with isopropyl alcohol (IPA) to eliminate any residual resin on their surface. This was followed by a UV irradiation post-cure for 30 minutes. Subsequently, the samples were soaked in IPA for 24 hours, and then in the 0.05 M PBS solution for an additional 24 hours. This ensured the removal of any unreacted monomers and allowed the samples to achieve equilibrium swelling.

For the evaluation of the EAHs' bending performance, two 30-gauge platinum wires served as the electrodes. These electrodes were spaced 50 mm apart with their tips submerged in the electrolyte solution, and the EAH sample was positioned in between them. An adjustable DC power supply delivered varying potentials to characterize the performance differences among samples with distinct compositions. The movements of EAHs were documented using a Sony A6400 digital camera, providing insights into the bending speed and curvature. The bending curvature was measured using the camera-captured optical images and measured on a computer with ImageJ (Figure 4a).

3. Results

For this study, systematic characterizations have been carried out by preparing and examining a series of resins with varying compositions, as tabulated in Table 1. Each entry highlights a different weight percentage composition of AA and 4-HBA (Figure 1a), allowing us to explore their combined effects on the resulting EAH properties. As the primary component, AA was selected for its inherent electroactuation capabilities due to the presence of carboxyl groups in AA facilitating ion migration in response to external electric fields. This ion migration generates osmotic pressure variations within the hydrogel network, resulting in swelling and bending [8] (Figure 1b). On the other hand, 4-HBA was chosen to tune the mechanical strength of the EAH. While it doesn't directly participate in the electroactuation process, 4-HBA is crucial for imparting the desired elasticity to the hydrogel [12]. This ensures that while the hydrogel is electroactively responsive, it is simultaneously flexible and mechanically robust for various applications [13]. The range of concentrations for AA and 4-HBA was selected to understand its influence on the electroactuation efficiency and mechanical strength and to optimize it for a wider array of applications.

To yield rapid 3D printing of EAHs, a home-built μCLIP was utilized (Figure 2a). By taking advantage of an oxygen-permeable membrane, oxygen molecules were introduced into the thin layer of resin above the membrane, resulting in a polymerization inhibition zone (dead zone) [14]. The presence of the dead zone allows the continuous, layer-less, and high-resolution fabrication of 3D structures in a timely manner. Unlike conventional techniques, μCLIP utilizes a photo-activated polymerization process, wherein a continuous sequence of UV light exposures promotes the polymerization of a liquid resin, producing the desired geometry without the necessity of stepwise layer polymerization. This feature allows the rapid production of intricate designs with smoother finishes and superior mechanical properties [15].

By carefully characterizing the printing parameters, the prepared resin can be used to produce intricate lattice structures via μCLIP (Figure 2b) in a timely manner, of which the printing speed can be up to 25 μm/s for all three resin compositions tested. This high-resolution structure, with fine features and consistent geometry, reinforces the potential of the proposed material combination in delivering mechanically robust and electroactive responsive EAHs. The resolution achieved, evident in the detailed lattice architecture (Figure 2b), stands as a testament to the capabilities of the μCLIP process when paired with the tunable resin formulation.

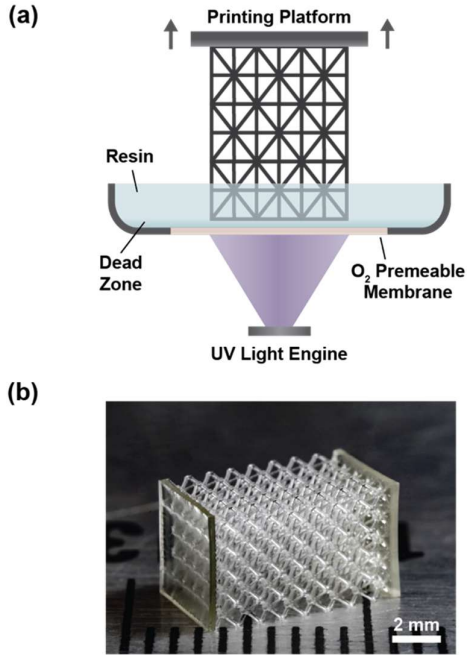

Figure 2. (a) Schematic illustration of home-built μCLIP system; (b) μCLIP produced octet lattice EAH structure using resin with 70 wt.% AA.

To reveal the effect of AA and 4-HBA concentrations on the mechanical strength of μCLIP printed EAH, tensile tests were performed on the μCLIP produced dog-bone samples with various resin compositions, as depicted in Figure 3a. The stress-strain curves presented in Figure 3b provide insight into the interplay between AA and 4-HBA concentrations. The EAH composed predominantly of AA, especially at a concentration of 70 wt.%, exhibits a peak stress threshold above 10 MPa at a strain of near 300%. This suggests its heightened load-bearing capacity under significant elongation, indicating a combination of strength and flexibility.

However, as AA concentration is decreased and the 4-HBA component increases, a clear reduction in the material's stress response at corresponding strain levels is observed. For instance, the sample with 30 wt.% AA demonstrates a substantially lower stress value even at higher strains. This inverse trend, arising from the increasing presence of 4-HBA, renders the hydrogel softer and more malleable, potentially enhancing its deformability under an applied load. The intricate relationship between stress and strain, influenced by the relative concentrations of AA and 4-HBA, is further emphasized in Figure 3c. Young's modulus of the samples shows a decreasing trajectory with increasing 4-HBA content, which confirmed its effect on increasing the elasticity of the

printing EAH. This underscores the inverse roles AA and 4-HBA that while AA contributes to robustness and resilience, 4-HBA imparts flexibility, striking a balance crucial for a wide range of applications.

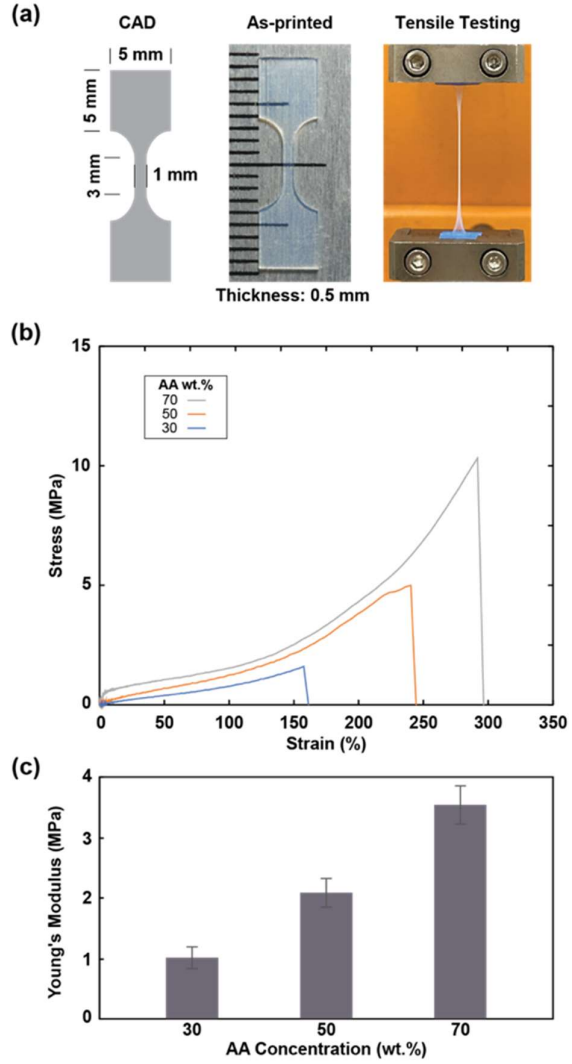

Figure 3. (a) CAD and μCLIP produced dog bone for tensile tests; (b) Strain-stress curves and (c) Young's modulus of as-printed EAH with varying resin compositions. (Error bars represent standard deviation, n = 5)

To elucidate the electroactive capabilities of the μCLIP printed EAHs, systematic tests were conducted in the presence of an electric field. EAH beams with a cross-section area of 0.5 × 0.5 mm and a length of 10 mm were printed for bending actuation tests. As illustrated in Figure 1b, samples were placed between the electrodes in 0.05 M PBS solution. Upon applying an electric field, the beams started to bend toward the cathode, and the maximum bending curvature was recorded for samples with varying compositions. The bending curvature was calculated as 1/R, where R is the radius of curvature, as shown in Figure 4a.

The bending performance of the EAHs, in relation to varying AA concentrations, is quantified in Figure 4b. At elevated electrical fields, the EAH sample with a high AA concentration (70 wt.%) shows the maximum bending curvature nearing 0.35 1/mm. As the AA concentration reduces, a direct and proportionate reduction in the maximum bending curvature is noted. While a more thorough study on an extended variety of resin compositions is demanded to better understand the bending behavior under different conditions, this trend still underscores the pivotal role of AA in influencing electroactive bending performance. The higher AA content augments the osmotic pressure within the hydrogel due to the presence of carboxyl groups, thereby enhancing the bending magnitude. Moreover, the increasing electric field has notably influenced the bending performance of the EAH. The bending curvatures corresponding to all three compositions clearly exhibit an upward trend with the escalation of the electrical field. Additionally, it is worth noting that exploring a broader range of electrical fields could further elucidate the numerical relationship between the compositions of EAHs and their actuation performance under varying conditions.

Furthermore, the time required for the EAH samples to attain their maximum bending curvature under varied electrical field strengths was characterized (Figure 4c). Irrespective of the AA concentration, all samples displayed an expedited response time with increasing electric field strengths. However, EAHs with higher AA concentrations, particularly at 70 wt.%, achieved their peak curvature in the shortest span, reinforcing the notion that AA concentration is intrinsically linked with rapid actuation responsiveness.

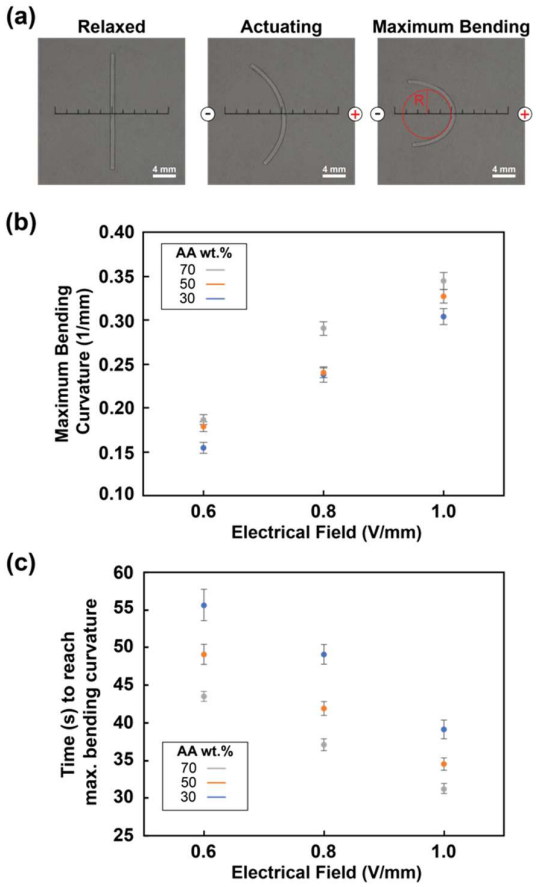

Figure 4. (a) Optical images of the EAH beam being actuated in the electrolyte; (b) Maximum bending curvature as a function of the electrical field strength; (c) Time to reach maximum bending curvature as a function of the electrical field strength. (Error bars represent standard deviation, n = 5)

In a quest to understand the temporal progression of the electroactuation of the μCLIP produced EAHs, bending curvature as a function of time for EAHs was formulated with varying AA concentrations under distinct electrical field strengths (Figure 5). A clear trend emerges across all AA concentrations that the bending curvature magnifies with elapsed time, eventually plateauing to reach a steady state at the maximum curvature. This suggests an initial acceleration phase of ion migration leading to the bending movement, which gradually stabilizes as the system approaches equilibrium. It can also be noted EAHs with higher AA concentrations, such as 70 wt.%, show a steeper gradient in their curvature progression, especially in the initial time intervals. This swift response can be attributed to the greater abundance of carboxyl groups, which enhance osmotic pressure and promote rapid actuation. Conversely, EAHs with lower AA concentrations exhibit a more gradual ascent, indicating a comparatively subdued electroactive response. Furthermore, the influence of the electrical field strength is significant within the expectation. At higher field strengths, such as 1 V/mm, the response of the EAHs is significantly enhanced across all resin formulations, which can be explained by expedited ion migration, culminating in a more vehement bending action.

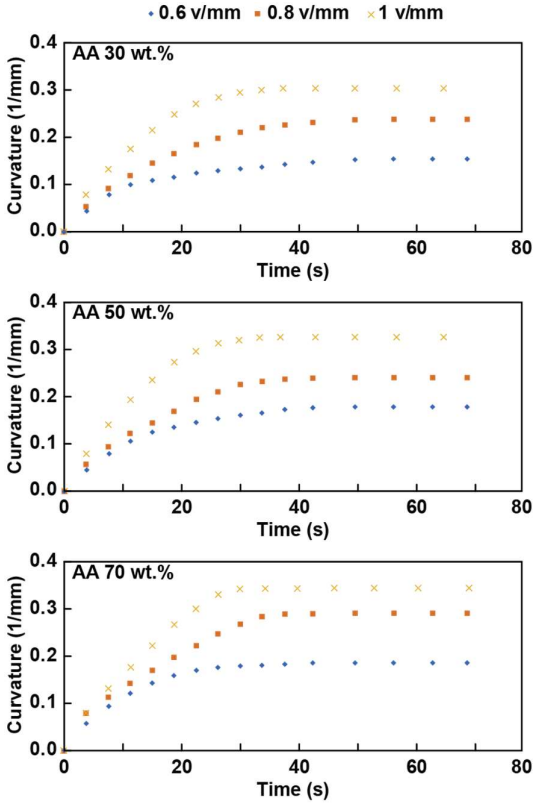

Figure 5. Bending curvature of EAH as a function of time under varying electrical field strength.

4. Summary

In this study, sophisticated electroactive hydrogel (EAH) was demonstrated to be suitable for rapid 3D printing via μCLIP system with photo resins, predominantly comprising AA and 4-HBA. The selection of AA was driven by its unparalleled electroactuation attributes, facilitated by the carboxyl groups, resulting in the characteristic bending of the hydrogel. In parallel, 4-HBA was incorporated to aid the mechanical resilience of the hydrogel. A series of characterizations have been performed to reveal not only the mechanical versatility of the EAHs but also their intricate electroactuation behavior. However, a more thorough characterization of EAHs composed of more comprehensive resin compositions is still required to better understand the impact on mechanical strength and bending behavior under varying conditions. The results will underscore the significant potential of these EAHs in a spectrum of advanced applications. These include soft robotics, where the tunable actuation can offer precise movements; wearable devices that require adaptable interfaces; targeted drug delivery systems, where the hydrogel's actuation can be employed for controlled release; and bioengineered tissues that could mimic natural biomechanics. The modifiability and high precision of the μCLIP produced EAHs ensure their viability in any application demanding nuanced and adjustable actuation responses.

Acknowledgements

This work was funded by National Science Foundation (NSF) Grant No. 2229279. The authors would like to thank Yuxiang Zhu and Prof. Kenan Song for coordinating with the DMA measurements.

References

[1] J. Kim et al., “Review of Soft Actuator Materials,” Int. J. Precis. Eng. Manuf., vol. 20, no. 12, pp. 2221–2241, Dec. 2019, doi: 10.1007/s12541-019-00255-1.

[2] N. El-Atab et al., “Soft Actuators for Soft Robotic Applications: A Review,” Advanced Intelligent Systems, vol. 2, no. 10, p. 2000128, 2020, doi: 10.1002/aisy.202000128.

[3] L. Kong et al., “Advances in preparation, design strategy and application of electroactive hydrogels,” Journal of Power Sources, vol. 581, p. 233485, Oct. 2023, doi: 10.1016/j.jpowsour.2023.233485.

[4] Y. Lee et al., “Hydrogel soft robotics,” Materials Today Physics, vol. 15, p. 100258, Dec. 2020, doi: 10.1016/j.mtphys.2020.100258.

[5] J. Kamcev et al., “Ion Activity Coefficients in Ion Exchange Polymers: Applicability of Manning’s Counterion Condensation Theory,” Macromolecules, vol. 48, no. 21, pp. 8011–8024, Nov. 2015, doi: 10.1021/acs.macromol.5b01654.

[6] M. L. O’Grady et al., “Optimization of Electroactive Hydrogel Actuators,” ACS Appl. Mater. Interfaces, vol. 2, no. 2, pp. 343–346, Feb. 2010, doi: 10.1021/am900755w.

[7] W. Wang et al., “High-Speed and High-Resolution 3D Printing of Self-Healing and Ion-Conductive Hydrogels via μCLIP,” ACS Materials Lett., vol. 5, no. 6, pp. 1727–1737, Jun. 2023, doi: 10.1021/acsmaterialslett.3c00439.

[8] M. A. Smirnov et al., “Electroactive hydrogels based on poly(acrylic acid) and polypyrrole,” Polym. Sci. Ser. A, vol. 53, no. 1, pp. 67–74, Jan. 2011, doi: 10.1134/S0965545X11010068.

[9] Y. Wang et al., “Poly(acrylic acid)-Based Hydrogel Actuators Fabricated via Digital Light Projection Additive Manufacturing,” ACS Appl. Polym. Mater., vol. 4, no. 2, pp. 971–979, Feb. 2022, doi: 10.1021/acsapm.1c01423.

[10] G. Kwon et al. "Electrically-driven hydrogel actuators in microfluidic channels: fabrication, characterization, and biological application." Lab on a Chip, vol. 10, no. 12, pp. 1604-1610, Apr. 2010, doi: 10.1039/B926443D.

[11] Z. Wang et al. "3D Printed Ultrasensitive Graphene Hydrogel Self-Adhesive Wearable Devices." ACS Applied Electronic Materials, vol. 4, no. 11, pp. 5199-5207, Apr. 2022, doi: 10.1021/acsaelm.2c00867.
[12] R. Luo et al., “Gradient Porous Elastic Hydrogels with Shape-Memory Property and Anisotropic Responses for Programmable Locomotion,” Advanced Functional Materials, vol. 25, no. 47, pp. 7272–7279, 2015, doi: 10.1002/adfm.201503434.
[13] G. Han Kwon et al., “Electrically-driven hydrogel actuators in microfluidic channels: fabrication, characterization, and biological application,” Lab on a Chip, vol. 10, no. 12, pp. 1604–1610, 2010, doi: 10.1039/B926443D.
[14] J. R. Tumbleston et al., “Continuous liquid interface production of 3D objects,” Science, Mar. 2015, doi: 10.1126/science.aaa2397.
[15] S. Liu et al., “Continuous Three-Dimensional Printing of Architected Piezoelectric Sensors in Minutes,” Research, vol. 2022, Jul. 2022, doi: 10.34133/2022/9790307.